J Solid State Electrochem (2008) 12:1173–1178
DOI 10.1007/s10008-008-0546-y

ORIGINAL PAPER

Synthesis of $Li[Li_{0.2}Ni_{0.2}Mn_{0.6}]O_2$ by radiated polymer gel method and impact of deficient Li on its structure and electrochemical properties

H. Y. Xu · Q. Y. Wang · C. H. Chen

Received: 26 June 2007 / Revised: 9 August 2007 / Accepted: 15 August 2007 / Published online: 6 May 2008

Abstract Layered $Li[Li_{0.16}Ni_{0.21}Mn_{0.63}]O_2$ and $Li[Li_{0.2}Ni_{0.2}Mn_{0.6}]O_2$ compounds were successfully synthesized by radiated polymer gel (RPG) method. The effect of deficient Li on the structure and electrochemical performance was investigated by means of X-ray diffraction, X-ray absorption near-edge spectroscopy and electrochemical cell cycling. The reduced Ni valence in $Li[Li_{0.16}Ni_{0.21}Mn_{0.63}]O_2$ leads to a higher capacity owing to faster Li^+ chemical diffusivity relative to the baseline composition $Li[Li_{0.2}Ni_{0.2}Mn_{0.6}]O_2$. Cyclic voltammograms (CV) and a simultaneous direct current (DC) resistance measurement were also performed on Li/$Li[Li_{0.16}Ni_{0.21}Mn_{0.63}]O_2$ and Li/$Li[Li_{0.2}Ni_{0.2}Mn_{0.6}]O_2$ cells. $Li[Li_{0.16}Ni_{0.21}Mn_{0.63}]O_2$ shows better electrochemical performance with a reversible capacity of 158 mA hg^{-1} at 1C rate at 20 °C.

Keywords Lithium nickel manganese oxide · Lithium deficiency · Cathode · Lithium battery

Introduction

Layered lithium nickel manganese oxide ($Li[Ni_xLi_{(1/3-2x/3)}Mn_{(2/3-x/3)}]O_2$, $0 \le x \le 1/2$) (LNM) series, with alternating lithium layers and transition metal rich layers separated by close-packed oxygen arrays, have recently been proved promising positive electrode materials for use in lithium-ion rechargeable batteries in recent years [1–15]. Ohzuku et al. showed that this material represents a possible alternative to $LiCoO_2$ for advanced lithium batteries, in terms of its operating voltage, capacity, cyclability, safety, and materials economy [1]. Meng et al. found that degree of nickel and lithium interlayer mixing (exchange) decreases as the nickel content x in $Li[Ni_xLi_{(1/3-2x/3)}Mn_{(2/3-x/3)}]O_2$ is reduced [15]. Therefore, the discharge capacity increases with increasing lithium content at the 3a sites in the layered Li–Ni–Mn–O compounds. The formal charges for the Ni and Mn of the material are Ni^{2+} and Mn^{4+}, respectively. Interestingly, only the $Ni^{2+/3+/4+}$ redox couples for $Li[Li_{0.2}Ni_{0.2}Mn_{0.6}]O_2$ are electrochemically available, and they are accompanied by Li^+ intercalation or deintercalation [2, 5, 10, 16]. On the other hand, the tetravalent Mn remains electrochemically inactive, but it provides significant structural stability with the strong Mn–O bonding. The electrochemical behavior of this electrode material is sensitive to nickel content, synthesis precursors, synthesis temperature, heat-treatment time, and cooling rates [2, 4, 7, 8], because these conditions lead to different cation arrangements in the layered structure.

So far, several chemical routes including composite carbonate process and sol–gel method have been used to synthesize LNM powders [8, 17, 18]. In our previous study, we have succeeded in preparing $LiCoO_2$ and $LiNi_{0.5}Mn_{1.5}O_4$ powders through a novel radiated polymer gel method (RPG) [19, 20]. In this method, the formation of the gel is quick and easy to control, and, most importantly, the precursors are mixed very homogeneously in the gel that can be transformed into a cathode powder after high-temperature calcination. Here we have applied the RPG method to successfully synthesize layered Li–Ni–Mn–O

H. Y. Xu · Q. Y. Wang · C. H. Chen (✉)
Laboratory for Advanced Functional Materials and Devices,
Department of Materials Science and Engineering,
University of Science and Technology of China,
Anhui Hefei 230026, People's Republic of China
e-mail: cchchen@ustc.edu.cn

H. Y. Xu
Department of Inorganic Non-metal Material Engineering,
Shandong University of Science and Technology,
Shandong Qingdao 266510, People's Republic of China

materials and investigated their structure and electrochemical properties.

Myung et al. recently reported that the electrochemical properties of $Li[(Ni_{0.5}Mn_{0.5})_{1-x}Li_x]O_2$ are enhanced by lithium excess [21]. As the excess amount of Li is located at the transition-metal layer and has significantly improved structural ordering in the crystal structure, the resulting electrochemical properties of $Li[(Ni_{0.5}Mn_{0.5})_{0.94}Li_{0.06}]O_2$ is superior to those of $Li[Ni_{0.5}Mn_{0.5}]O_2$. Shlyakhtin et al. also reported similar results in the same system [22]. However, Ceder et al. recently reported that low-valent transition metal could greatly help to facilitate lithium ion diffusion by a reduction of activation energy of Li migration for layered cathode materials [23], which is propitious to improve the electrochemical properties of cathode materials. It is expected that the valence of the transition mental would decrease with deficient amount of Li for LNM powders, which maybe bring excellent electrochemical performance. Thus, in the present study, we investigate and discuss for the first time the effects of the deficient amount of Li relative to the baseline composition $Li[Li_{0.2}Ni_{0.2}Mn_{0.6}]O_2$ on the structure and electrochemical properties of LNM powders.

Experimental

$LiNO_3$, $Ni(NO_3)_2{\cdot}6H_2O$ and $Mn(CH_3COO)_2{\cdot}4H_2O$ were dissolved in deionized water in the molar ratio of Ni/Mn= 1/3 and Li:(Ni^+ Mn)=1.5,1.6, respectively, to obtain 0.5 M solutions. Then acrylic acid (AA) (CH_2=CHCOOH) was added to form AA–H_2O (1:2 *v*/*v*) solutions, the pH value of which was about 2. The solutions were polymerized under the condition of ^{60}Co γ-ray irradiation (intensity 55–75 Gy/min) for 5 h. Thus, a green and homogeneous poly (acrylic acid) gel was obtained. The gel was heated at 140 °C for 5 h to get rid of the impregnated water and AA residue. A subsequent heat treatment was carried out at 900 °C in air for 12 h, and then both samples were quenched to room temperature. The chemical compositions of the resulting powders were analyzed by inductively coupled plasma and atomic emission spectroscopy (ICP-AES; Atomscan Advantage). The particle size distribution of the oxide powder was determined with a laser particle analyzer (LPA; Rise-2006).

The crystalline structure of the samples was characterized by X-ray diffraction (XRD) using a diffractometer (Philips X'Pert Pro Super, CuKα radiation). The diffraction patterns were recorded at room temperature in the 2θ range from 10 to 75 °C. The average oxidation-state of Ni and Mn was determined by the iodometry titration. In this analysis, Li–Ni–Mn–O powder was first dissolved in a dilute hydrochloric acid solution. The reductions of Mn^{4+}, Mn^{3+} to Mn^{2+} and Ni^{3+} to Ni^{2+} were achieved by adding excess amount of KI solid into the solution, forming I_3^-. Back titration for the resulting I_3^- was carried out by a $Na_2S_2O_3$ solution with a predetermined concentration (0.01 M). Thus, the average oxidation state of Ni and Mn can be calculated. In addition, the Ni and Mn K-edge X-ray absorption near edge structure (XANES) analysis was also used to study the local structure of the synthesized Li–Ni–Mn–O powders. The XANES data were collected from the XAFS station of Hefei National Synchrotron Radiation Laboratory.

Electrode laminates for the electrochemical testing were prepared by casting slurry consisting of Li–Ni–Mn–O powder (84 wt%), acetylene black (8 wt%), and poly (vinylidene fluoride) (PVDF) (8 wt%) dispersed in 1-methyl-2-pyrrolidinone (NMP) onto an aluminum foil. The laminates were then dried at 70 °C for 2 h. The Li/$Li_{1.1}Ni_{0.2}Mn_{0.6}O_2$ or Li/$Li_{1.2}Ni_{0.2}Mn_{0.6}O_2$ coin-cells (2032 size) were made with 1 M $LiPF_6$ in ethylene carbonate (EC): diethyl carbonate (DEC) (1:1 *w*/*w*) as the electrolyte. The cells were tested on a multi-channel battery cycler (Shenzhen Neware Co.) and subjected to charge–discharge cycles at C/5, 1C rate between 2.0 and 4.8 V, respectively (vs Li metal) in the constant current constant voltage (CCCV) mode at 20 °C around.

Cyclic voltammograms of these cells were measured on a CHI604B Electrochemical Workstation from 2.0 to 5.0 V at a scanning rate of 0.2 mV/s. The internal resistance of the cells was also measured by a current interruption technique. This was done by cutting off the current intermittently for 1 min through the process of charge and recording the voltage change before and after interruption. Thus, the direct current (DC) resistance of a cell (R_{dc}) at a certain state-of-charge (SOC) can be calculated as $R_{dc}=\Delta U/\Delta I$.

Results and discussion

Composition and structure analysis

Considering the fact that a small portion of lithium evaporation occurs during a high temperature heat treatment [24], the starting ratio of Li/[Ni^+ Mn] was decided to be 1.5 and 1.6 in this study. The ICP-AES analysis shows that calcination of the radiated polymer gel powders (Li/[Ni^+ Mn]=1.5 and 1.6, respectively) at 900 °C for 12 h in air results in a less-stoichiometry of lithium sample $Li_{1.1}Ni_{0.2}Mn_{0.6}O_{2-\delta}$ and a stoichiometric sample $Li_{1.2}Ni_{0.2}Mn_{0.6}O_2$. It is reasonable to assume that without any electrochemical delithiation there is no appreciable ionic vacancy in the as-sintered LNM powders. Then the formula of the two samples can be rewritten as $Li[Li_{0.16}Ni_{0.21}Mn_{0.63}]O_2$ (less-stoichiometry of Li composition) and $Li[Li_{0.2}Ni_{0.2}Mn_{0.6}]O_2$ (baseline composition), respectively.

The X-ray diffraction patterns of $Li[Li_{0.16}Ni_{0.21}Mn_{0.63}]O_2$ and $Li[Li_{0.2}Ni_{0.2}Mn_{0.6}]O_2$ powders, with Miller indices indication, are presented in Fig. 1. Layered structure with high crystallinity is formed, and all the peaks can be indexed based on a hexagonal α-$NaFeO_2$ structure with space group *R3 m*, except for some weak peaks around 20°. These weak peaks are caused by super-lattice ordering of the Li, Ni, and Mn ions in the transition-metal layers [8, 18, 25]. Here, we show that the single phase of $Li[Li_{0.16}Ni_{0.21}Mn_{0.63}]O_2$ and $Li[Li_{0.2}Ni_{0.2}Mn_{0.6}]O_2$ with well-layered structure can be easily prepared by the RPG method without any repeated calcination steps. In addition, as shown at the top right corner of Fig. 1, the Bragg diffraction-angles turn to lower direction for $Li[Li_{0.16}Ni_{0.21}Mn_{0.63}]O_2$. Based on these XRD patterns, the lattice parameters and cell volume can be calculated by the Unit Cell software based on the least-square method. The result is shown in Table 1. It is obvious that the lattice parameters *a*, *c* and cell volume all increase for $Li[Li_{0.16}Ni_{0.21}Mn_{0.63}]O_2$. However, the ratio of *c*/*a* remained the same as that of baseline sample, and the reason is not clear in the present study.

It is also expected that Ni valence in the compound becomes lower for $Li[Li_{0.16}Ni_{0.21}Mn_{0.63}]O_2$ compared to $Li[Li_{0.2}Ni_{0.2}Mn_{0.6}]O_2$ if the manganese valence remains^{+} 4. The iodometry titration results show that the average oxidation states of mixed Ni and Mn in $Li[Li_{0.16}Ni_{0.21}Mn_{0.63}]O_2$ and $Li[Li_{0.2}Ni_{0.2}Mn_{0.6}]O_2$ are 3.31 and 3.54, respectively. In fact, the average oxidation states of mixed Ni and Mn should be 3.5 with Ni^{2+} and Mn^{4+}. Hence, we can deduce that there are Mn^{3+} in $Li[Li_{0.16}Ni_{0.21}Mn_{0.63}]O_2$ and Ni^{3+} in $Li[Li_{0.2}Ni_{0.2}Mn_{0.6}]O_2$. To confirm this, the K-edge XANES spectra of Ni and Mn are shown in Fig. 2. Though lacking in reference sample, it is clear that the nickel valence in Li

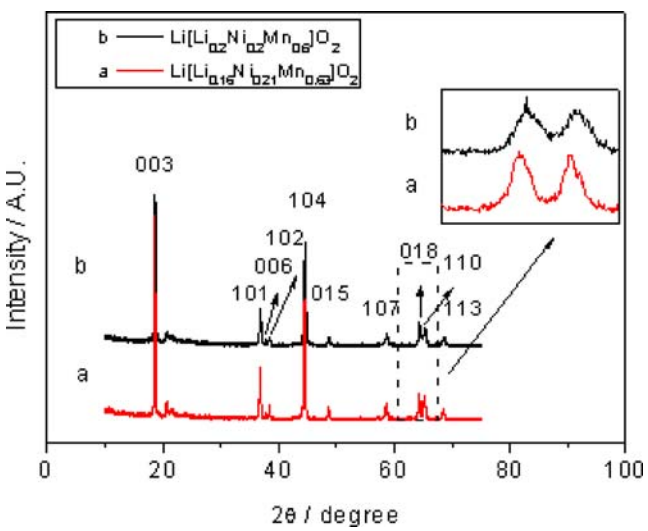

Fig. 1 X-ray diffraction patterns of $Li[Li_{0.16}Ni_{0.21}Mn_{0.63}]O_2$ and $Li[Li_{0.2}Ni_{0.2}Mn_{0.6}]O_2$ having *R3 m* space group

$[Li_{0.16}Ni_{0.21}Mn_{0.63}]O_2$ is apparently lower than that in $Li[Li_{0.2}Ni_{0.2}Mn_{0.6}]O_2$ (Fig. 2a) while the manganese valence keeps changeless (Fig. 2b). So, it is clear that oxidation states of Mn for both compounds were less than 4^{+}, and the distinction of average valence of Ni and Mn was mainly caused by different Ni oxidation states. This is likely why the lattice parameters of $Li[Li_{0.16}Ni_{0.21}Mn_{0.63}]O_2$ increase compared with $Li[Li_{0.2}Ni_{0.2}Mn_{0.6}]O_2$ (Table 1).

The particle size distribution (PSD) profiles of the $Li[Li_{0.16}Ni_{0.21}Mn_{0.63}]O_2$ and $Li[Li_{0.2}Ni_{0.2}Mn_{0.6}]O_2$ powders are given in Fig. 3. The powders exhibit a narrow size distribution with a median particle size D50 of 0.6 μm and D99 of 1.8 μm, which means 50 wt% of the powder is smaller than 0.6 μm and 99 wt% of the powder is smaller than 1.8 μm in particle size for both samples. The relatively small particle size ensures a short length of Li diffusion pathways from its position in the Li–Ni–Mn–O lattice to the cathode–electrolyte interface, which promotes a faster and uniform Li intercalation into Li–Ni–Mn–O crystallites during charge–discharge process.

Electrochemical performance

Cyclic voltammograms (CV) of $Li[Li_{0.16}Ni_{0.21}Mn_{0.63}]O_2$/Li and $Li[Li_{0.2}Ni_{0.2}Mn_{0.6}]O_2$/Li cells in the first cycle are given in Fig. 4. They show a pair of reversible intercalation/deintercalation peaks around 4.0–4.1 V and 3.7–3.8 V, respectively, and an irreversible deintercalation peak around 4.8 V. Dahn et al. [3] found that $Li/Li[Ni^{2+}{}_xLi_{(1/3-2x/3)}Mn^{4+}{}_{(2/3-x/3)}]O_2$ cells give smooth reversible voltage profiles with the higher cut-off voltage below 4.45 V when 2*x* Li atoms per formula unit are removed. The Ni oxidation state is below 4^{+}, and reversible intercalation is observed as expected. If the cells are charged to higher voltages, they exhibit a high-voltage plateau between 4.5 and 4.7 V (equal to 1−2*x* lithium amount). They also found that when the charge potential was increased to 4.8 V an irreversible plateau occurs that corresponds to the simultaneous extraction of both Li and O from the materials, which resulted in a special oxygen deficient material that may contribute extra capacity due to the charge–discharge reversibility after the first charge to 4.8 V [3]. This means that the total deintercalation capacity in the first cycle (C_{tot}) can be divided into two parts: the capacity associated with the increase of Ni valence (C_{Ni}) and that associated with the deintercalation of oxygen (C_{Oxy}), i.e. $C_{tot}=C_{Ni}+C_{Oxy}$. In our studied two compositions $Li[Li_{0.16}Ni_{0.21}Mn_{0.63}]O_2$ and $Li[Li_{0.2}Ni_{0.2}Mn_{0.6}]O_2$, the theoretical C_{Ni} and C_{Oxy} can be calculated as $C_{Ni}=0.20*(4-V_{Ni})$, $C_{Oxy}=1-0.20*(4-V_{Ni})$ and $C_{Ni}=0.21*\left(4-V_{Ni}^{'}\right)$, $C_{Oxy}=1-0.21*\left(4-V_{Ni}^{'}\right)$, respectively. As analyzed above, the oxidation states of Ni (V_{Ni}) for $Li[Li_{0.16}Ni_{0.21}Mn_{0.63}]O_2$ is lower than that of Li $[Li_{0.2}Ni_{0.2}Mn_{0.6}]O_2$ $\left(V_{Ni}^{'}\right)$, so the ratio of C_{Ni}/C_{Oxy} for Li

Table 1 Calculated lattice parameters by unit cell software based on the least-square method

Sample	*a*-axis	*c*-axis	*c*/*a*	Unit volume
	Å	Å		Å^3
$Li[Li_{0.16}Ni_{0.21}Mn_{0.63}]O_2$	2.8633	14.222	4.967	100.97
$Li[Li_{0.2}Ni_{0.2}Mn_{0.6}]O_2$	2.8597	14.203	4.966	100.58

$[Li_{0.16}Ni_{0.21}Mn_{0.63}]O_2$ is bigger than that of baseline composition. This result is qualitatively consistent with the peak area relationship of the two deintercalation steps as shown in the cyclic voltammograms (Fig. 4). It is also noticed that the peak separation of $Li[Li_{0.16}Ni_{0.21}Mn_{0.63}]O_2$/Li cell is narrower than that of $Li[Li_{0.2}Ni_{0.2}Mn_{0.6}]O_2$/Li cell during reversible charge and discharge stage. This difference should be related to the polarization effect due to the variation of cell impedance, which will be further discussed in the following paragraph.

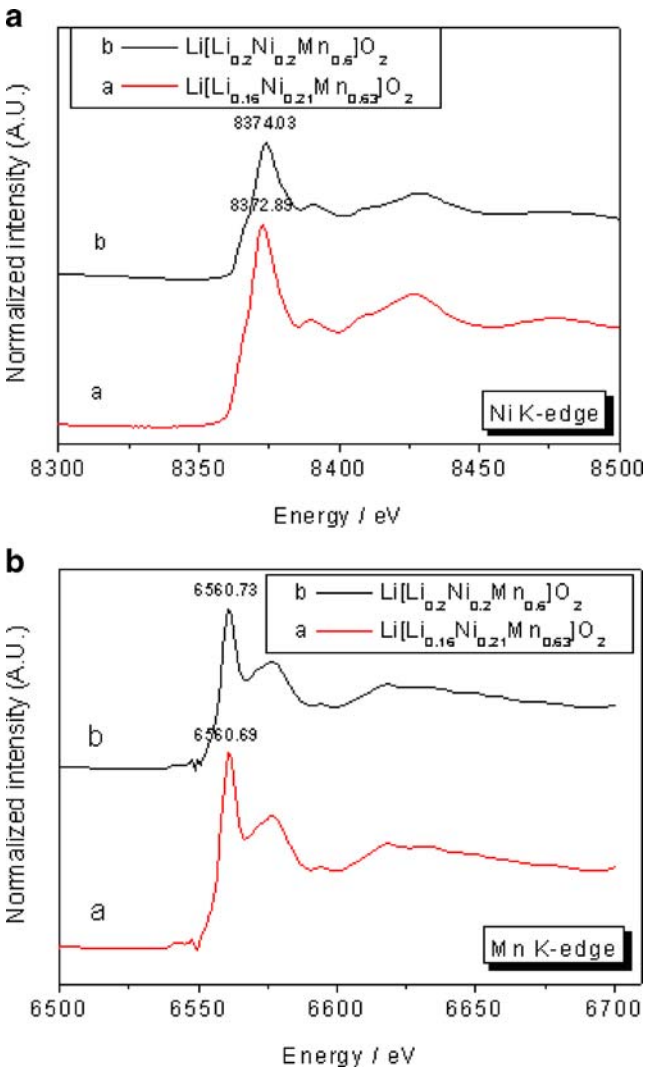

Fig. 2 Ni (**a**) and Mn (**b**) K-edge XANES spectra for Li–Ni–Mn–O powders

The charge–discharge profiles of Li/$Li[Li_{0.16}Ni_{0.21}Mn_{0.63}]O_2$ and Li/$Li[Li_{0.2}Ni_{0.2}Mn_{0.6}]O_2$ cells cycled between 2.0 and 4.8 V at 30 °C with C/5 rate at 30th cycle are presented in Fig. 5. It can be seen that both of the cells made with Li $[Li_{0.16}Ni_{0.21}Mn_{0.63}]O_2$ and $Li[Li_{0.2}Ni_{0.2}Mn_{0.6}]O_2$ electrodes reveal a 4.0 V plateau. Li/$Li[Li_{0.16}Ni_{0.21}Mn_{0.63}]O_2$ cell delivers higher overall capacity (190 mAhg^{-1}) than Li/Li $[Li_{0.2}Ni_{0.20}Mn_{0.60}]O_2$ cell (154 mA hg^{-1}) does. According to above analysis on C_{tot}, the theoretical capacity for Li/Li $[Li_{0.16}Ni_{0.21}Mn_{0.63}]O_2$ cell with all Li extracted from the Li layers is around 334 mA hg^{-1}. This means that the lithium is still not completely extracted during the electrochemical cycling. Furthermore, it is noticed that its discrepancy between the charge and discharge voltage plateaus is less than that of Li/$Li[Li_{0.2}Ni_{0.2}Mn_{0.6}]O_2$ cells, which means small polarization in $Li[Li_{0.16}Ni_{0.21}Mn_{0.63}]O_2$. This result is consistent with the CV data, which has been discussed above. As analyzed above using XANES, we know that the average Ni valence of deficient lithium sample is lower than that of the baseline composition, which means that $Li[Li_{0.16}Ni_{0.21}Mn_{0.63}]O_2$ is less oxidizing than Li $[Li_{0.2}Ni_{0.2}Mn_{0.6}]O_2$. Therefore, less amount of surface layer due to the oxidation of the electrolyte is probably formed on $Li[Li_{0.16}Ni_{0.21}Mn_{0.63}]O_2$ than on $Li[Li_{0.2}Ni_{0.2}Mn_{0.6}]O_2$. Hence, it is expected that the impedance of Li/$Li[Li_{0.16}Ni_{0.21}Mn_{0.63}]O_2$ cells is lower than that of Li/Li $[Li_{0.2}Ni_{0.2}Mn_{0.6}]O_2$ cells. Also, Ceder et al. recently reported low-valent transition mental could greatly help to increase

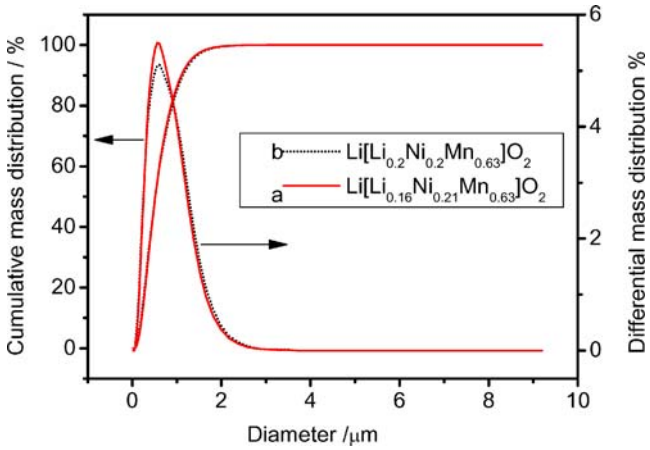

Fig. 3 Particle size distribution of the $Li[Li_{0.16}Ni_{0.21}Mn_{0.63}]O_2$ and Li $[Li_{0.2}Ni_{0.2}Mn_{0.6}]O_2$ powders clacined at 900 °C for 12 h

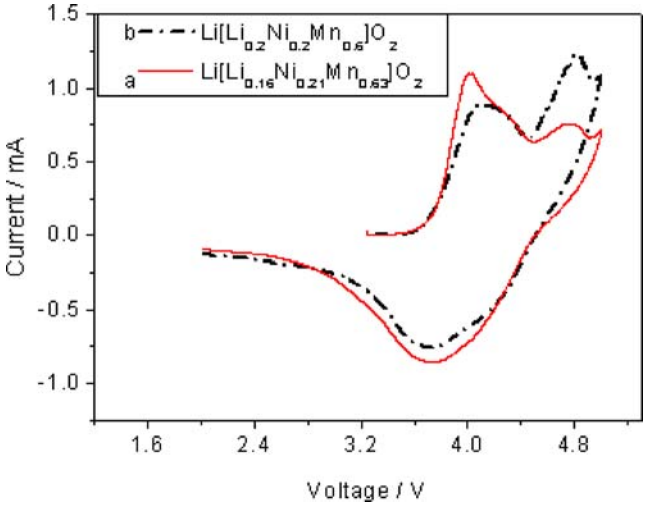

Fig. 4 Cyclic voltammograms of $Li[Li_{0.16}Ni_{0.21}Mn_{0.63}]O_2$ and $Li[Li_{0.2}Ni_{0.2}Mn_{0.6}]O_2$ cells with 1 M $LiPF_6$/EC+DEC as the electrolyte. Scan rate was 0.02 mV/s

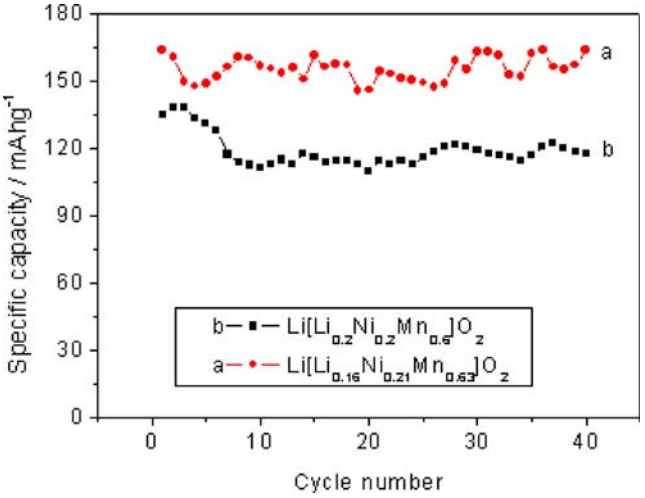

Fig. 6 1C-rate discharge capacity of $Li[Li_{0.16}Ni_{0.21}Mn_{0.63}]O_2$ and $Li[Li_{0.2}Ni_{0.2}Mn_{0.6}]O_2$ cells vs cycle number

lithium ion diffusion by a reduction of activation energy of Li migration for layered cathode materials [23]. Thus, all of above three factors should lead to an improvement of high rate capacity for $Li[Li_{0.16}Ni_{0.21}Mn_{0.63}]O_2$ sample, which is discussed in the following paragraph.

The discharge capacity vs cycle number for the Li/Li $[Li_{0.16}Ni_{0.21}Mn_{0.63}]O_2$ and Li/$Li[Li_{0.2}Ni_{0.2}Mn_{0.6}]O_2$ cells in the voltage range 2.0–4.8 V at 1C rate is given in Fig. 6. After some fluctuation in the first few cycles, the discharge capacity of the two electrodes reaches rather stable values of 158 and 117 mA hg^{-1}, respectively, after about ten cycles. In literature, the electrochemical properties of Li $[Li_{0.2}Ni_{0.2}Mn_{0.6}]O_2$ are mostly focused on lower discharge rate [18, 26, 27]. Park et al. studied the change of discharge capacity at different specific densities and they obtained about 130 mA hg^{-1} at 1C-rate between 2.0 and 4.8 V (vs Li metal) at 21 °C [25], which is substantially lower than the capacity obtained here for $Li[Li_{0.16}Ni_{0.21}Mn_{0.63}]O_2$. Therefore, the cell with $Li[Li_{0.16}Ni_{0.21}Mn_{0.63}]O_2$ electrode delivers a steady and high capacity at 1C rate and the charge–discharge efficiency is found over 98% during the cycling. From the results of the study by Park et al., we also found that the specific capacity of this material was obviously different when the test temperature was changed by 10 °C [25]. It is probably the reason of the capacity fluctuation for both of samples as shown in Fig. 6, although the Li- deficient sample seems to show more fluctuation. The excellent electrochemical performance of $Li[Li_{0.16}Ni_{0.21}Mn_{0.63}]O_2$ is originated from faster lithium ion diffusion in the cathode material due to the lower Ni valence and thinner surface electrolyte interface (SEI) layer on the cathode. The less-stoichiometry of lithium sample indeed can improve high rate (1C here) capacity of layered Li–Ni–Mn–O material. According to the above discussions, the influence of lithium

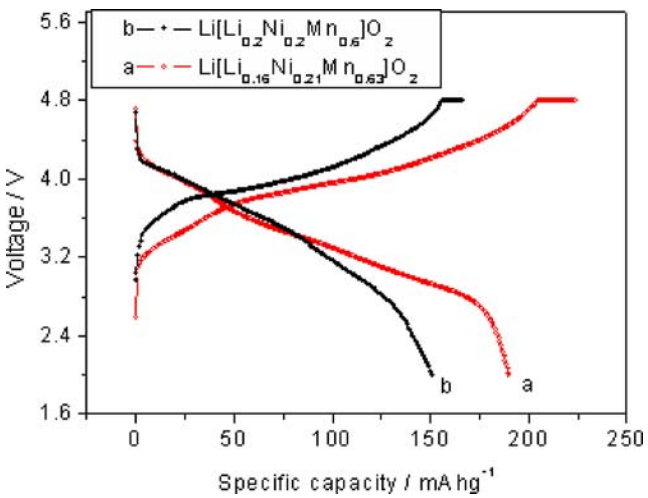

Fig. 5 Charge–discharge curves for $Li[Li_{0.16}Ni_{0.21}Mn_{0.63}]O_2$ and $Li[Li_{0.2}Ni_{0.2}Mn_{0.6}]O_2$ cells at their 30th cycle. The discharge rate was C/5

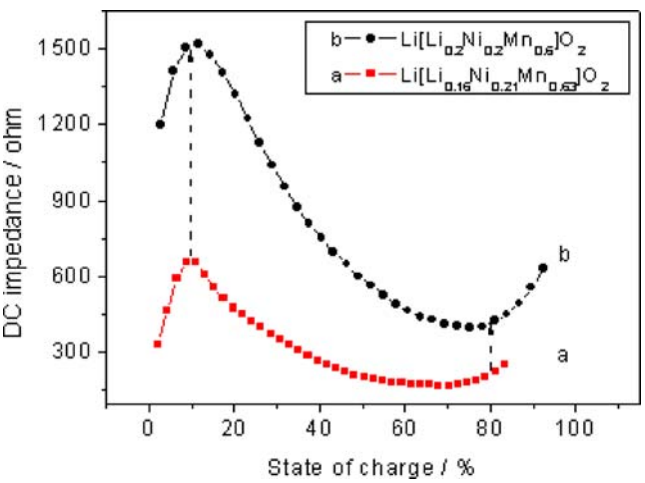

Fig. 7 The direct current resistance of $Li[Li_{0.16}Ni_{0.21}Mn_{0.63}]O_2$ and $Li[Li_{0.2}Ni_{0.2}Mn_{0.6}]O_2$ cells as a function of the state of charge

diffusion effect should increase with growing discharge rates. Comparing the capacity ratio of 1C to C/5 rate of two samples at the 30th cycle, it is about 86 to 77% for Li/Li $[Li_{0.16}Ni_{0.21}Mn_{0.63}]O_2$ and Li/Li$[Li_{0.2}Ni_{0.2}Mn_{0.6}]O_2$ cells, respectively.

Figure 7 shows the DC resistance of the cells vs the state-of-charge (SOC). Obviously, Li/Li$[Li_{0.16}Ni_{0.21}Mn_{0.63}]O_2$ cell demonstrates significantly lower resistance than Li/Li$[Li_{0.2}Ni_{0.2}Mn_{0.6}]O_2$ cell does during the whole charge state. This is consistent with the above analysis about the SEI layer impedance and lithium diffusivity in the lattice. In fact, the presence of more Ni^{2+} in $Li[Li_{0.16}Ni_{0.21}Mn_{0.63}]O_2$ should also increase the intrinsic electronic conductivity of the cathode. This is probably one of the main reasons why the difference of the cell impedance in the beginning stage of charge step is markedly greater than in the later stage of charge step (Fig. 7).

Conclusions

The 4.0 V-cathode $Li[Li_{0.16}Ni_{0.21}Mn_{0.63}]O_2$ and $Li[Li_{0.2}Ni_{0.2}Mn_{0.6}]O_2$ powders with a narrow particle size distribution have been prepared with radiated polymer gel method. $Li[Li_{0.16}Ni_{0.21}Mn_{0.63}]O_2$ shows excellent electrochemical performance with a high reversible 1C-rate capacity of 158 mA hg^{-1} in the voltage range of 2.0 to 4.7 V. The presence of lower Ni oxidation state in $Li[Li_{0.16}Ni_{0.21}Mn_{0.63}]O_2$ plays an important role in facilitating the lithium diffusivity, enhancing the electronic conductivity, and suppressing the surface layer resistance. This deficient lithium of LNM is very promising as a potential cathode material for lithium secondary batteries.

Acknowledgements This study was supported by National Science Foundation of China (grant No. 50372064 and 20471057). We are also grateful to the China Education Ministry (SRFDP No. 20030358057). The USTC radiation chemistry laboratory has provided the assistance for the polymer gel synthesis. Hefei National Synchrotron Radiation Laboratory has assisted in collecting the XANES data.

References

1. Ohzuku T, Makimura Y (2001) Chem Lett 30:744
2. Lu ZH, Macneil DD, Dahn JR (2001) Electrochem Solid State Lett 4:A191
3. Lu ZH, Dahn JR (2002) J Electrochem Soc 149:A815
4. Lu ZH, Beaulien LY, Donaberger RA, Thomas CL, Jahn JR (2002) J Electrochem Soc 149:A778
5. Yoon WS, Pack Y, Yang XQ, Balasubramanian M, Mebreen J, Grey CP (2002) Electrochem Solid State Lett 5:A263
6. Reed J, Ceder G (2002) Electrochem Solid State Lett 5:A145
7. Makimura Y, Ohzuku T (2003) J Power Sources 119:3214
8. Lu ZH, Chen ZH, Dahn JR (2003) Chem Mater 15:3214
9. Johnson CS, Kim JS, Kropf AJ, Kahaian AJ, Vaughey JT, Fransson LM, Thackeray MM (2003) Chem Mater 15:2313
10. Yoon WS, Grey CP, Balasubramanian M, Yang XQ, Mebreen J (2003) Chem Mater 15:3161
11. Grey CP, Yoon WS, Reed J, Ceder G (2004) Electrochem Solid State Lett 7:A290
12. Meng YS, Ceder G, Grey CP, Yoon WS (2004) Electrochem Solid State Lett 7:A155
13. Yoon WS, Iannopollo S, Grey CP, Carlier D, Reed J, Ceder G (2004) Electrochem Solid State Lett 7:A167
14. Kim JS, Johnson CS, Vaughey JT, Thackeray MM, Hachney SA (2004) Chem Mater 16:1996
15. Meng YS, Ceder G, Grey CP, Yoon WS, Jiang M, Breger J, Shao-Horn Y (2005) Chem Mater 17:2386
16. Arachi Y, Kobayachi H, Emura S, Nakata Y, Tanaka M, Asai T (2003) Chem Lett 32:60
17. Shin SS, Sun YK, Amine K (2002) J Power Sources 112:634
18. Hwang BJ, Wang CJ, Chen CH, Tsai YW, Venkateswarlu M (2005) J Power Sources 146:658
19. Ding N, Ge XW, Chen CH (2005) Mater Res Bull 40:1451
20. Xu HY, Xie S, Ding N, Liu BL, Shang Y, Chen CH (2006) Electrochim Acta 51:4352
21. Myung ST, Komaba S, Kurihara K, Hosoya K, Kumagai N, Sun YK, Nakai I, Yonemura M, Kamiyama T (2006) Chem Mater 18:1658
22. Shlyakhtin OA, Choi SH, Yoon YS, Oh YJ (2005) J Power Sources 141:122
23. Kang K, Meng YS, Breger J, Grey CP, Ceder G (2006) Science 311:977
24. Myung ST, Komaba S, Kumagai N (2002) Solid State Ionics 150:199
25. Park YJ, Hong YS, Wu X, Chang SH (2004) J Power Sources 129:288
26. Kang SH, Sun YK, Amine K (2003) Electrochem Solid State Lett 6:A183
27. Kim JH, Sun YK (2003) J Power Sources 119:166